Toward electrochemical synthesis of cement—An electrolyzer-based process for decarbonating $CaCO_3$ while producing useful gas streams

Leah D. Ellis[a], Andres F. Badel[a], Miki L. Chiang[a], Richard J.-Y. Park[a], and Yet-Ming Chiang[a,1]

[a]Department of Material Science and Engineering, Massachusetts Institute of Technology, Cambridge, MA 02139

Edited by Richard Eisenberg, University of Rochester, Rochester, New York, and approved August 2, 2019 (received for review March 15, 2019)

Cement production is currently the largest single industrial emitter of CO_2, accounting for ∼8% (2.8 Gtons/y) of global CO_2 emissions. Deep decarbonization of cement manufacturing will require remediation of both the CO_2 emissions due to the decomposition of $CaCO_3$ to CaO and that due to combustion of fossil fuels (primarily coal) in calcining (∼900 °C) and sintering (∼1,450 °C). Here, we demonstrate an electrochemical process that uses neutral water electrolysis to produce a pH gradient in which $CaCO_3$ is decarbonated at low pH and $Ca(OH)_2$ is precipitated at high pH, concurrently producing a high-purity O_2/CO_2 gas mixture (1:2 molar ratio at stoichiometric operation) at the anode and H_2 at the cathode. We show that the solid $Ca(OH)_2$ product readily decomposes and reacts with SiO_2 to form alite, the majority cementitious phase in Portland cement. Electrochemical calcination produces concentrated gas streams from which CO_2 may be readily separated and sequestered, H_2 and/or O_2 may be used to generate electric power via fuel cells or combustors, O_2 may be used as a component of oxyfuel in the cement kiln to improve efficiency and lower CO_2 emissions, or the output gases may be used for other value-added processes such as liquid fuel production. Analysis shows that if the hydrogen produced by the reactor were combusted to heat the high-temperature kiln, the electrochemical cement process could be powered solely by renewable electricity.

cement | electrolysis | decarbonization | hydrogen | carbon dioxide

As discussed at the 2018 Sackler Colloquium "Status and Challenges in Science for Decarbonizing our Energy Landscape" and in other recent analyses (1–4), deep decarbonization of today's energy system will require addressing not only energy generation (24% of global greenhouse gas emissions) and transportation (14% of global greenhouse gas emissions) but also difficult-to-decarbonize sectors such as large industry, which today is responsible for about 21% of global greenhouse gas emissions (5). Industry uses fossil fuels for heat and to drive chemical and thermochemical reactions but may become less reliant on fossil fuel if 1) electrical alternatives become available and 2) the cost and reliability of renewable electricity continues to improve (6, 7). The rise of very low-cost renewable electricity has already motivated the search for electrochemical methods to innovate industrial processes (1, 8, 9). Among these, electrochemical pathways to the production of cement have heretofore been limited; 1 previous example is high-temperature electrochemical decarbonation using molten salts, operating in the same temperature range as thermal calciners (10, 11). Here, we propose and demonstrate proof of concept for an ambient-temperature electrochemically based process that decarbonates $CaCO_3$, precipitates solid $Ca(OH)_2$ from which desired calcium silicates are synthesized, and produces concentrated gas streams of H_2 and O_2 + CO_2 that are amenable to CO_2 capture and sequestration, and/or used in other value-added processes (Fig. 1).

Portland cement (12) is the most widely produced man-made material in the world, produced at a rate of 4 billion metric tons per year (13). Excluding agriculture, cement production is the largest industrial source of greenhouse gases (steelmaking follows closely), accountable today for 8% of global greenhouse gas emissions (14). About one-half of the emitted CO_2 is due to the use of $CaCO_3$ (generally, limestone) as a key component, with the balance being mainly due to combustion of fossil fuels in the cement kiln (15). Demand for cement is growing as the world's population increases and becomes more urban, and as emerging economies develop infrastructure (16). By 2060, the number of buildings on Earth is expected to double; this is equivalent to building a New York City each 30 days for the next 40 years (17). Since each kilogram of cement produced emits nearly 1 kg of CO_2 (15), several gigatons of CO_2 per year will be released from new infrastructure, highlighting the urgency of decarbonizing cement production.

Current efforts to reduce cement's carbon footprint include carbon capture from flue gases, use of alternative fuels, or development of supplementary cementitious materials (14, 18–21). Currently, the flue gas from cement plants is too impure for economical carbon capture through amine scrubbing; use of alternative fuels (such as used tires) does not alleviate the primary emissions from $CaCO_3$; and use of supplementary materials in the concrete has limited impact on the carbon emissions from Portland cement and may simultaneously compromise the physical properties (14, 19–21). Another family of approaches uses the cement to capture and sequester more CO_2, producing a carbonate-enriched cement or concrete product (22–25). In contrast with the above approaches, we were motivated to seek electrochemically based approaches that have the potential to produce the most widely accepted and used cements, thereby minimizing adoption risk, while taking advantage of emerging very low-cost renewable electricity to alleviate both the chemical and thermal sources of CO_2. As we show, our process can work synergistically with other scientific and technological tools of a sustainable energy system discussed in the Sackler Colloquium, including wind and solar electricity, water splitting and fuel creation, and chemical and electrical energy storage.

Our reactor takes advantage of the inherent pH gradients in an electrolysis cell to carry out $CaCO_3$ decarbonation and $Ca(OH)_2$ precipitation and collection (Fig. 2). We show that the $Ca(OH)_2$ produced in this manner, which requires less energy to dehydrate

This paper results from the Arthur M. Sackler Colloquium of the National Academy of Sciences, "Status and Challenges in Decarbonizing our Energy Landscape," held October 10–12, 2018, at the Arnold and Mabel Beckman Center of the National Academies of Sciences and Engineering in Irvine, CA. NAS colloquia began in 1991 and have been published in PNAS since 1995. From February 2001 through May 2019 colloquia were supported by a generous gift from The Dame Jillian and Dr. Arthur M. Sackler Foundation for the Arts, Sciences, & Humanities, in memory of Dame Sackler's husband, Arthur M. Sackler. The complete program and video recordings of most presentations are available on the NAS website at http://www.nasonline.org/decarbonizing.

Author contributions: L.D.E. and Y.-M.C. designed research; L.D.E., A.F.B., M.L.C., and R.J.-Y.P. performed research; L.D.E., A.F.B., and Y.-M.C. analyzed data; and L.D.E., A.F.B., and Y.-M.C. wrote the paper.

Conflict of interest statement: Y.-M.C., L.D.E., and A.F.B. are inventors on patent applications filed by Massachusetts Institute of Technology in relation to certain subject matter in the paper.

This article is a PNAS Direct Submission.

See online for related content such as Commentaries.

[1]To whom correspondence may be addressed. Email: ychiang@mit.edu.

This article contains supporting information online at www.pnas.org/lookup/suppl/doi:10.1073/pnas.1821673116/-/DCSupplemental.

First published September 16, 2019.

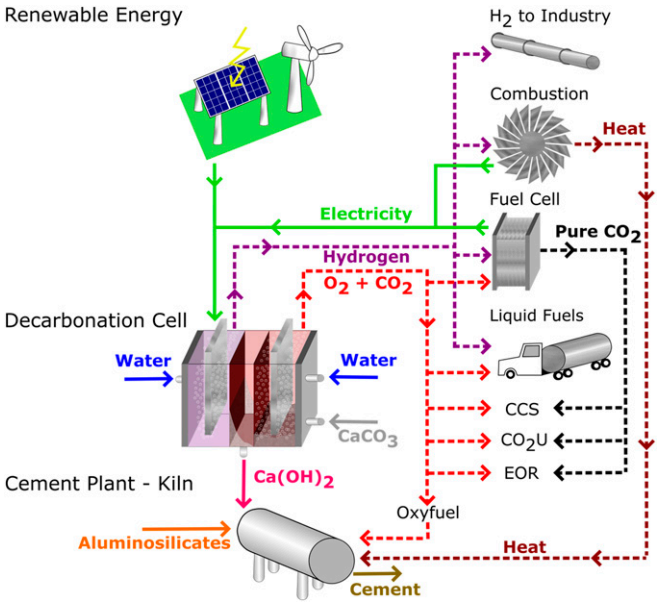

Fig. 1. Scheme for a low-emission, electrochemically based cement plant. An electrochemical decarbonation reactor powered by renewable electricity converts $CaCO_3$ to $Ca(OH)_2$ for use in cement synthesis. The decarbonation cell (Fig. 2) uses the pH gradient produced by neutral-water electrolysis to dissolve $CaCO_3$ at the acidic anode and precipitate $Ca(OH)_2$ where pH ≥ 12.5. Simultaneously, H_2 is generated at the cathode and O_2/CO_2 are generated at the anode. These gas streams can serve several alternative roles in a sustainable production system. CO_2 can be directly captured from the inherently concentrated stream (CCS). Electricity or heat can be generated from the H_2 and O_2 via fuel cells or combustors. The O_2/CO_2 oxy-fuel can be recirculated to the kiln for cleaner combustion in the cement sintering cycle. CO_2 reuse and utilization (CO_2U) concepts can be employed, such as use in EOR or production of liquid fuels.

to CaO than is required to calcine $CaCO_3$, is readily reacted with SiO_2 to produce alite, the major active phase (50 to 70% by weight) in Portland cement (12). Near-stoichiometric operation, where every 2 protons electrolytically produced at the oxygen-generating anode decarbonates 1 $CaCO_3$ formula unit, is demonstrated at laboratory scale. We propose several pathways by which this electrochemical decarbonation reactor can be integrated into a low- or zero-carbon-emission cement plant (Fig. 1), including powering by renewable electricity and using the gases produced in any of several alternative functions such as 1) direct capture and sequestration of the inherently concentrated CO_2 stream, 2) generation of electricity or heat from the H_2 (and optionally the O_2) via fuel cells or combustors, 3) providing oxy-fuel for cleaner combustion in the cement sintering cycle, and 4) liquid fuel production. A first-order technoeconomic analysis of the energy consumption and fuel cost of such a process as a function of the cost of renewable electricity is presented.

Results

Our decarbonation cell simultaneously functions as an electrolyzer as well as chemical reactor to convert solid $CaCO_3$ to solid $Ca(OH)_2$, illustrated schematically in Fig. 2 and demonstrated experimentally in Fig. 3 and *SI Appendix*, Figs. S2 and S3. An electrolyzer operating with near-neutral water has the following anode and cathode half-cell reactions:

$$2H_2O \rightarrow O_2 + 4H^+ + 4e^- \quad [1]$$

$$2H_2O + 2e^- \rightarrow H_2 + 2OH^-. \quad [2]$$

At steady state, the electrolyzer produces a pH gradient that is readily visualized upon addition of universal pH indicator to an operating H-cell, as shown in Fig. 3 and Movies S1 and S2. In such an electrolyzer, H^+ and OH^- will normally recombine to form water:

$$H^+ + OH^- \rightarrow H_2O. \quad [3]$$

Our reactor replaces this reaction with a decarbonation reaction. When $CaCO_3$ is added to the acidic solution produced in the vicinity of the anode during electrolysis, chemical decarbonation occurs via the following sequence of reactions (26):

$$(K = 6 \times 10^{-9}) \quad CaCO_{3(s)} \rightleftharpoons Ca^{2+}_{(aq)} + CO^{2-}_{3(aq)} \quad [4]$$

$$(K = 2.1 \times 10^{10}) \quad CO_3^{2-} + H^+ \rightleftharpoons HCO_3^- \quad [5a]$$

$$(K = 2.2 \times 10^{6}) \quad HCO_3^- + H^+ \rightleftharpoons H_2CO_3 \quad [5b]$$

$$(K = 5.9 \times 10^{2}) \quad H_2CO_{3(aq)} \rightleftharpoons CO_{2(g)} + H_2O. \quad [5c]$$

Dissolved Ca^{2+} (Eq. **4**) is drawn towards the anode and then precipitates from solution as $Ca(OH)_2$ upon reaction with OH^-; this reaction is favored above pH 12.5:

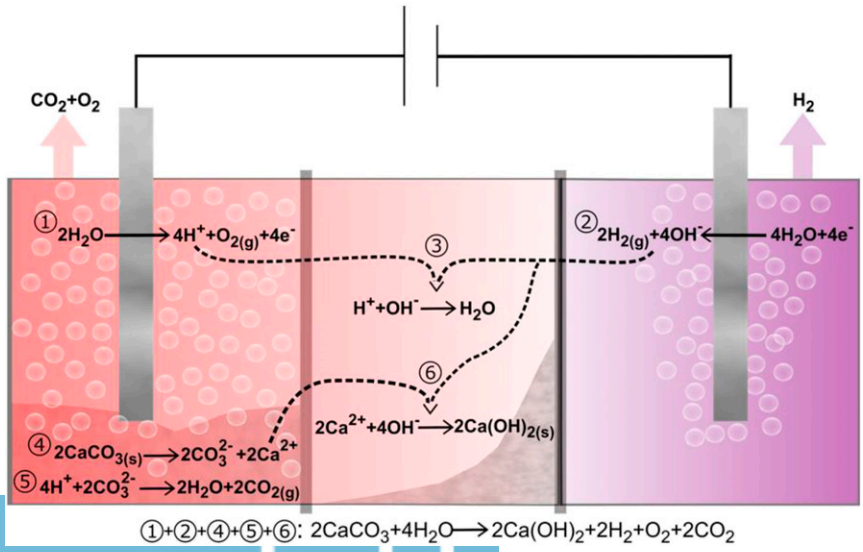

Fig. 2. Schematic of electrolyzer-based decarbonation cell. Reactions 1 and 2 are oxygen evolution and hydrogen evolution half-cell reactions respectively, under near-neutral pH. Reaction 3 is formation of water from its component ions. Reactions 4 and 5 represent decomposition of calcium carbonate and release of CO_2; see the text for intermediate steps. In reaction 6, hydroxide ions in reaction 3 instead go toward formation of calcium hydroxide, and protons protonate carbonate ions (reaction 5). The overall reaction in which $CaCO_3$ is converted to $Ca(OH)_2$ with attendant release of H_2, O_2, and CO_2 is shown at the bottom.

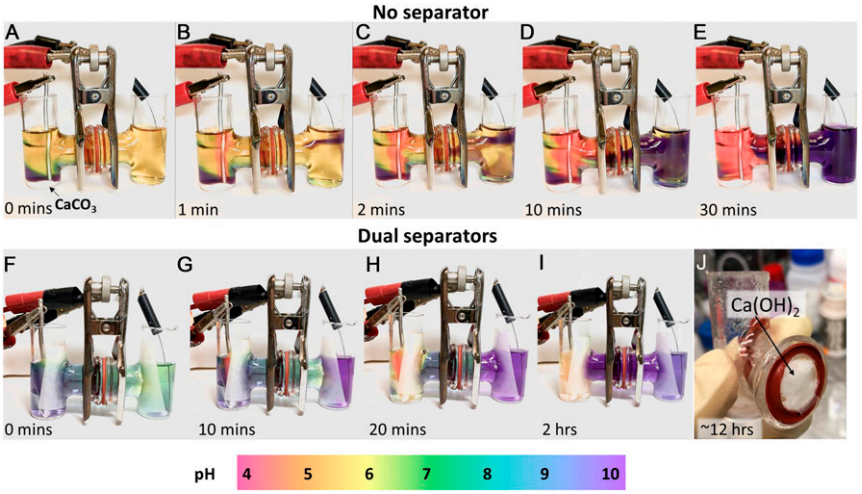

Fig. 3. Time-lapse images of decarbonation H-cells using platinum electrodes and 1 M $NaNO_3$ in deionized water as electrolyte. Each cell contains a few drops of pH indicator dye, for which the color scale is shown at the bottom. (*A–E*) Cell containing $CaCO_3$ powder in the anode (left) chamber and with no porous separator between chambers. Electrolysis at 2.5-V cell voltage (~6-mA current) produces color gradient showing acidic solution at anode (left) and alkaline solution at cathode (right). Close examination of cross-tube shows stratification of the solutions, attributed to density-driven convection. (*F–I*) Decarbonation cell in which porous fiber separators are used at both chambers to restrict convection, and $CaCO_3$ powder source is contained within a removable cup so that weight loss can be monitored. Note absence of stratification. (*J*) $Ca(OH)_2$ precipitated in cross-tube after 12 h of electrolysis at a high cell voltage of 9 V to accelerate reaction.

$$Ca^{2+} + 2OH^- \rightarrow Ca(OH)_2. \quad [6]$$

The sum of the electrochemical and chemical reactions occurring in the cell is

$$2CaCO_{3(s)} + 4H_2O_{(l)} \rightarrow 2Ca(OH)_{2(s)} + 2H_{2(g)} + O_{2(g)} + 2CO_{2(g)}. \quad [7]$$

We define stoichiometric operation of this reactor as the condition where every 2 mol of protons produced during electrolysis (Eq. **1**) converts 1 mol of $CaCO_3$ to 1 mol of $Ca(OH)_2$ as shown in Eq. **7**; this represents the maximum possible yield and coulombic efficiency. At stoichiometric operation, the ratio of gases produced is also given by Eq. **7**: each mole of $Ca(OH)_2$ produced results in the generation of 1 mol of H_2 at the cathode and 1 mol of O_2 and 2 mol of CO_2 at the anode.

Previously, Rau, along with others (27–30), proposed using electrolytic decarbonation, powered by renewable electricity, as a means of mitigating ocean acidification. Their concept is in turn similar to the operation of a calcium reactor used to maintain alkalinity in reef aquariums: $CaCO_3$ is reacted with acid (in Rau's case, the acid is made from the oxidation of seawater) to produce dissolved $Ca(HCO_3)_2$ and $Ca(OH)_2$ at the cathode. The resulting solution of $Ca(HCO_3)_2$ and $Ca(OH)_2$ is alkaline and captures CO_2 from the atmosphere to reform $CaCO_3$ and can be returned to the saltwater body to mitigate acidification. Here, instead of using electrolytic decarbonation for CO_2 capture, we liberate the CO_2 as a gaseous product to be captured and sequestered, or used in other processes, and precipitate the $Ca(OH)_2$ for use in cement production. Note that in addition to cement production, $Ca(OH)_2$ is an important component in the manufacture of refined sugar, pulp and paper, alkali carbonates, for wastewater remediation, and as a fluxing agent in steel refining (31). Typically the $Ca(OH)_2$ is produced by slaking of CaO obtained by calcination of $CaCO_3$; using our decarbonation reactor, $Ca(OH)_2$ could be produced directly for these applications as well, while allowing direct capture of the CO_2 produced.

A series of laboratory H-cell reactors was constructed to test the proposed scheme. Fig. 3 *A–E* shows time-lapse images of a reactor assembled with platinum electrodes and using an electrolyte consisting of 1 M $NaNO_3$ in distilled water, to which a few drops of universal pH indicator have been added. The color scale correlating color to pH is shown at the bottom of the figure. The anode chamber contains $CaCO_3$ powder, and in contrast to the cell in Fig. 3 *F–J*, no porous separator is used between the chambers. Initially, in Fig. 3*A* the yellow tint shows that the electrolyte is at pH ~6 everywhere except immediately above the bed of $CaCO_3$ powder, where the purple tint shows that partial dissolution of the carbonate has raised the pH to >10. Fig. 3 *B–E* show the cell at different times after electrolysis commences, under potentiostatic conditions (2.5-V cell voltage, ~6-mA current). The color gradients show that over time a steeper pH gradient develops, reaching more extreme pH values in each chamber, consistent with the half-cell reactions (Eqs. **1** and **2**). However, close examination of the solution within the cross-tube shows a distinct stratification, with the acidic (pink) solution above and the alkaline (purple) solution below, which we attribute to a density difference between the 2 solutions. Movie S1 shows the development of the pH gradient and stratified liquid layers in this cell over time. In this cell configuration, $Ca(OH)_2$ was observed to precipitate across the length of the cell including directly on the platinum wire cathode, which it eventually passivates. As shown in *SI Appendix*, Fig. S1, passivation leads to a sharp drop in cell current after a few hours of operation.

Fig. 3 *F–I* show the same cell design but with a porous paper separator placed at the intersection of each chamber with the cross-tube in order to limit convection. In addition, the $CaCO_3$ powder source in this cell is contained within a removable cup so that the dissolution of $CaCO_3$ as a function of time could be measured by removing and weighing the remaining powder (after drying). Note the lack of stratification; in the absence of convective mixing the cells could be operated for >12 h without $Ca(OH)_2$ passivation of the cathode (*SI Appendix*, Fig. S1). In this cell the alkaline solution diffuses as a uniform front across the cell, and at steady-state operation the pH within the cross-tube is high enough that $Ca(OH)_2$ precipitation occurs predominantly between the separators, where it is readily collected for analysis. Note also that in this configuration the pH around the anode is far less acidic (i.e., no pink tint), and in fact the yellow color indicates pH ~6. This is significant because 6 is approximately the pH at which HCO_3^- and $CO_{2(aq)}$ are in equilibrium. The observation suggests that essentially all of the protons produced in the oxygen

evolution reaction (Eq. **1**) are consumed by reaction with the carbonate ion (Eq. **5**). We confirm this through independent measurements discussed later. In addition, the composition of the output gases was confirmed by gas chromatography.

Using the cell design in Fig. 3 *F*–*I*, we collected significant amounts of white precipitate on the porous paper separator directly in front of the cathode, as shown in Fig. 3*J*. Upon drying, the precipitate was confirmed using powder X-ray diffraction (XRD) to be predominantly $Ca(OH)_2$ with a small amount of $CaCO_3$ (6%, based on Rietveld refinement) (Fig. 4*A*). Brunauer–Emmett–Teller (BET) analysis showed that the precipitate has a specific surface area of 0.8 m^2/g. The impurity $CaCO_3$ may have formed upon exposure of the $Ca(OH)_2$ to air when preparing samples for XRD, or when some of the soluble HCO_3^- deprotonates on contact with OH^- to reform $CaCO_3$. Scanning electron microscopy (SEM) shows that the $Ca(OH)_2$ particles are crystallized with 3 different characteristic length scales. The largest isolated crystallites (Fig. 4*B*) have dimensions of tens of micrometers and show a hexagonal prism morphology characteristic of $Ca(OH)_2$ (32). Next in size scale are aggregates of much finer crystallites having dimensions of a few micrometers (Fig. 4 *C* and *D*) but of similar hexagonal-prism morphology. Finally, there exist precipitates with a rounded nodule morphology, which at higher magnification reveals submicrometer-scale crystallites (Fig. 4 *E* and *F*). The appearance of 3 different morphologies of $Ca(OH)_2$ precipitates suggests that nucleation and growth conditions vary widely within the reactor. The origin of these variations is a topic for future study. However, essentially all of the particles produced fall below the <90-μm specification typical for raw mixes in cement production (12). Composition analysis by energy-dispersive X-ray analysis (*SI Appendix*, Fig. S2) showed no impurities above background levels in the $Ca(OH)_2$ except for trace amounts of Na, likely resulting from the Na salt used in the reactor electrolyte. Thus, the present approach appears to be capable of producing fine, high-purity $Ca(OH)_2$ particulates.

A series of experiments was conducted to characterize the coulombic efficiency of the reactor compared to the stoichiometric limit. In each experiment, an H-cell reactor was assembled with fresh electrolyte, using 1 M of either $NaClO_4$ or $NaNO_3$ salt, and the same starting amount of $CaCO_3$ powder. The reactor was operated under potentiostatic conditions (3.5 V) for times from 1 to 14 h, after which the $CaCO_3$-containing cup was removed from the reactor, dried, and weighed to obtain the amount of $CaCO_3$ lost to chemical dissolution. Results from 13 experiments are plotted in Fig. 5 as the moles of dissolved $CaCO_3$ against the coulombs passed (upper abscissa), obtained by integrating the current over the duration of the experiment, and the H_2 gas equivalent (lower abscissa), calculated assuming that the rate of electrolysis is equal to the cell current (i.e., no side reactions). The red dashed line in Fig. 5 represents the stoichiometric reaction wherein every 2 protons produced at the anode in the oxygen-evolving reaction protonates 1 carbonate ion. The error bars for each data point correspond to cumulative weighing error based on the precision of the scale. A least-squares fit through all of the data points yields a ratio of chemical reaction rate to electrolysis rate of 0.85, relative to a maximum value of 1. This demonstrates that a high coulombic efficiency is possible, even using an unoptimized laboratory-scale reactor. For both electrolytes the longest-time data (far right data points) show a fall-off in efficiency, which other experiments (*SI Appendix*, Fig. S1) suggest is due to passivation of the cathode with $Ca(OH)_2$ at long reactor run times. Note that some of the data points lie above the line of maximum theoretical efficiency. We attribute this deviation to some inadvertent loss of $CaCO_3$ during removal of the $CaCO_3$-containing cup from the reactor. We also attempted to measure directly the amount of $Ca(OH)_2$ produced in these experiments but were not able to recover all of the $Ca(OH)_2$ precipitated in the cells (e.g., from the cell walls) or to efficiently remove all of the precipitate on the paper separator. Clearly, more advanced reactors can be designed in which there is greater control over convection and chemical gradients, and in which the precipitated $Ca(OH)_2$ is collected more efficiently, including continuously. Such reactor design improvements are beyond the scope of the current paper. Even so, the present efficiency is close to the thermal efficiency of a conventional cement precalciner, which decarbonates about 90% of the incoming $CaCO_3$.

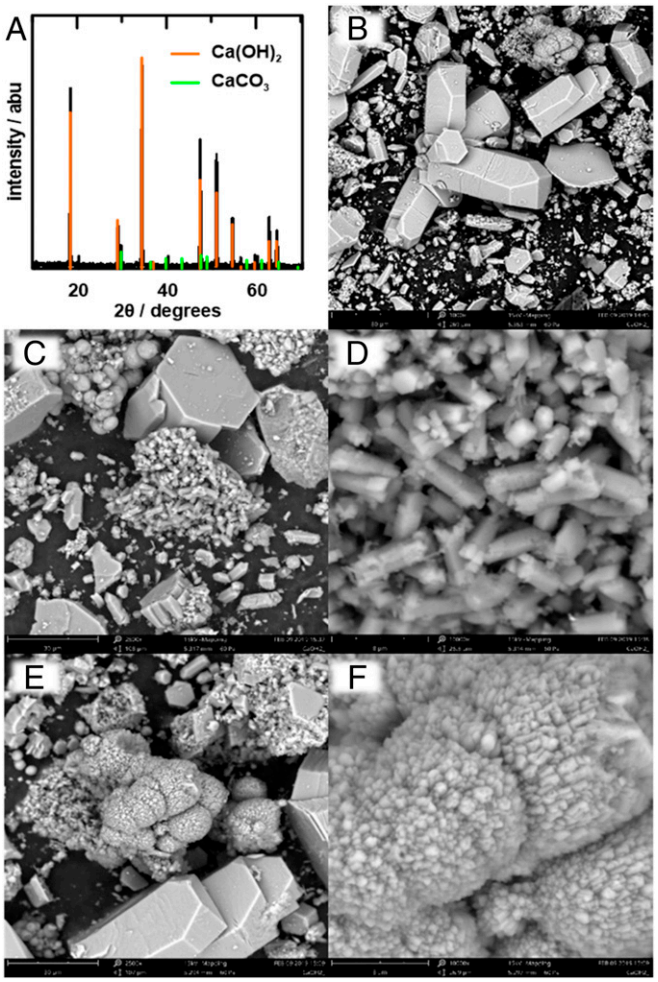

Fig. 4. $Ca(OH)_2$ powder produced by decarbonation reactor. (*A*) Powder XRD pattern from typical sample; Rietveld refinement shows 94% $Ca(OH)_2$ and 6% $CaCO_3$. (*B*–*F*) SEM imaging shows $Ca(OH)_2$ crystallites of 3 length scales. (*B*) Largest $Ca(OH)_2$ crystallites have tens-of-micrometers dimensions and characteristic hexagonal-prism morphology. (*C*) Aggregates of smaller $Ca(OH)_2$ crystalites, shown at higher magnification in *D*, have similar hexagonal-prism morphology but are of micrometer dimensions. (*E*) $Ca(OH)_2$ with rounded nodule morphology, which at higher magnification (*F*) shows submicrometer-scale crystallites.

Having demonstrated the efficacy of the proposed decarbonation reactor, we turned our attention to evaluating the suitability of its solid $Ca(OH)_2$ product as a precursor to Portland cement. The most abundant mineral in Portland cement, constituting 50 to 70% by weight, is alite, $3CaO{\cdot}SiO_2$. We prepared mixtures of the $Ca(OH)_2$ and a fine SiO_2 powder, as well as a control sample using purchased $CaCO_3$ powder mixed with the same SiO_2, in the 3:1 alite molar ratio. The mixed powders were subjected to heat treatment over a wide range of temperatures. Fig. 6 *A* and *B* show the XRD pattern and SEM image of the $Ca(OH)_2 + SiO_2$ mixture after heating to 600 °C for 2 h in air. Unlike $CaCO_3$, which does not decompose until 898 °C (at 1 atm P_{CO2}), $Ca(OH)_2$ has a thermodynamic decomposition temperature of 512 °C (at 1 atm P_{H2O}) and here has already decomposed to CaO upon firing at 600 °C, although the CaO

has not yet reacted with SiO_2 to form alite. After heating for 2 h at 1,500 °C, a typical cement kiln temperature, and cooling by turning off the furnace power, the mixture has reacted to form the low-temperature T1 polymorph of alite (ICSD:4331), as shown by the XRD pattern in Fig. 6*C*. The polymorphism of alite is known to depend on the nature and amount of impurities in the raw material as well as the cooling rate from kiln temperature (33). While the high-temperature M1 and M2 polymorphs are more commonly obtained in commercial processes, the T1 polymorph we obtained in slow-cooled samples is considered just as cementitious (33–35). Fig. 6*D* shows that the alite particles produced from our precursors are less than 30 μm in size, which is within the range desired for commercial Portland cements (12). Fig. 6 *E* and *F* show calcium and silicon composition maps, from which the compositional homogeneity of the alite is evident. Fig. 7 *A* and *B* show the XRD pattern and SEM image of the corresponding $CaCO_3$ and SiO_2 mixture after heating to 600 °C for 2 h in air, and Fig. 7 *C* and *D* show the results after heating to 800 °C for 2 h in air. At 600 °C, no significant decomposition has occurred, whereas at 800 °C the $CaCO_3$ has decomposed to CaO but reaction to alite has not commenced. After heating to 1,500 °C for 2 h (Fig. 7 *E* and *F*), the XRD shows that the alite phase has formed. However, there remains some unreacted CaO, 6% according to Rietveld refinement of the XRD spectra. The SEM image in Fig. 7*F*, when compared to Fig. 6*D*, shows that the $Ca(OH)_2$- and $CaCO_3$-derived alites ultimately reach similar particle morphologies and sizes. These results show that the electrochemically produced $Ca(OH)_2$ from our decarbonation reactor is a suitable precursor for synthesizing the main hydrating calcium silicate phase in Portland cement. Moreover, due to the fine precipitate morphology (compared to, for example, ground limestone) and its >300 °C lower decomposition temperature, it appears to have improved reactivity compared to $CaCO_3$, which could translate to reduced firing times and/or temperatures that lower energy consumption in the high-temperature reaction step.

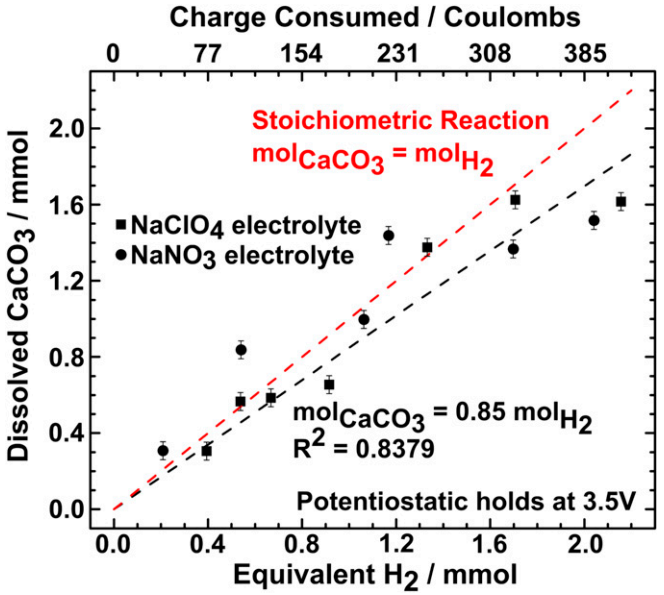

Fig. 5. Coulombic efficiency of the decarbonation reactor, measured from 13 experiments each starting with a freshly assembled H-cell of type in Fig. 2. Mass loss of $CaCO_3$ due to dissolution is plotted vs. total charge passed through system (top abscissa) and equivalent moles of hydrogen produced at cathode (lower abscissa), calculated assuming all current goes toward electrolysis. The red dashed line represents the stoichiometric reaction giving maximum conversion efficiency on a charge basis, and the black dashed line represents a least-squares fit to the data, the slope of which corresponds to ~85% coulombic efficiency.

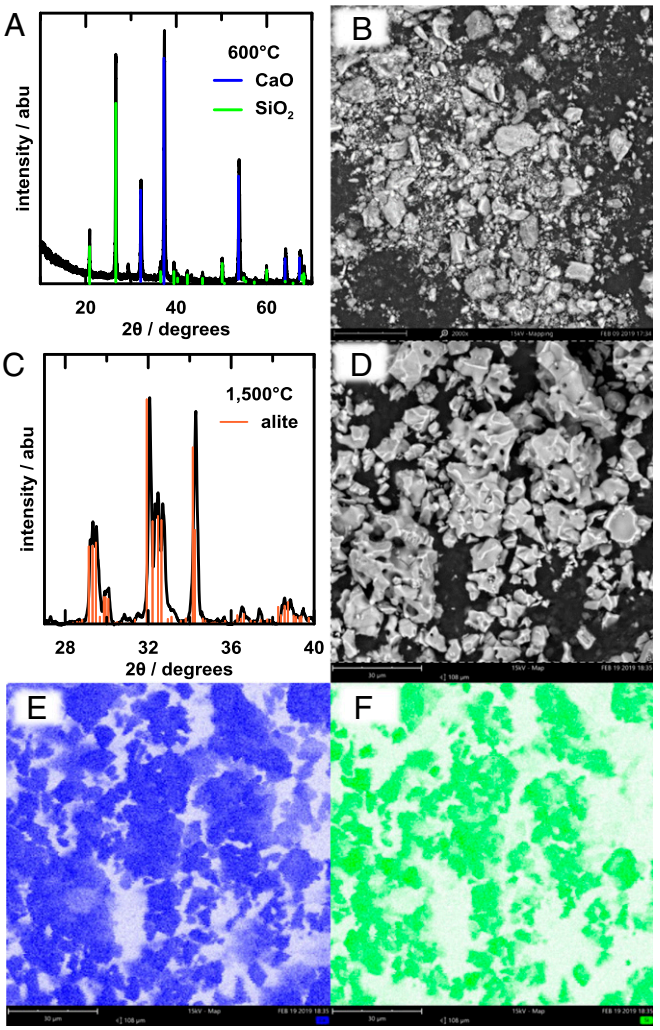

Fig. 6. Synthesis of alite, 3CaO-SiO_2, using $Ca(OH)_2$ produced in decarbonation reactor. (*A*) XRD pattern and (*B*) SEM image of mixture of $Ca(OH)_2$ and SiO_2 after heating to 600 °C for 2 h in air. The $Ca(OH)_2$ has decomposed to CaO but has not yet reacted with the SiO_2 to form the alite phase. After firing at 1,500 °C for 2 h, (*C*) XRD pattern shows single-phase alite, the morphology of which is shown in the SEM image in *D*. Composition maps (*E* and *F*) of calcium and silicon, respectively, show uniform distribution of both elements.

Discussion

In addition to producing a reactive $Ca(OH)_2$ suitable for cement synthesis, our electrolysis-based decarbonation reactor produces concentrated gas streams of H_2 at the cathode and O_2 and CO_2 (in a 1:2 molar ratio when operating at high coulombic efficiency) at the anode. These gases are important components in a wide range of sustainable technologies that are currently being pursued worldwide and open up several possible synergies between cement production and these technologies, which we now discuss.

Carbon capture and sequestration (CCS) at the cement plant level has to date focused on postcombustion capture of CO_2, combined with the use of oxy-fuel combustion. The O_2/CO_2 stream from our decarbonation reactor can make these processes simpler and more efficient. Postcombustion capture refers to technologies that capture CO_2 from the kiln exhaust, such as calcium looping, amine scrubbing, and membrane filtration (36–38). Oxy-fuel, or oxygen-enhanced combustion, refers to the burning of fossil fuels (here, primarily coal) with oxygen instead of air (37, 39). Oxy-combustion first results in improved fuel efficiency, since the nitrogen content of air does not have to be heated. Second, the absence of nitrogen permits higher flame

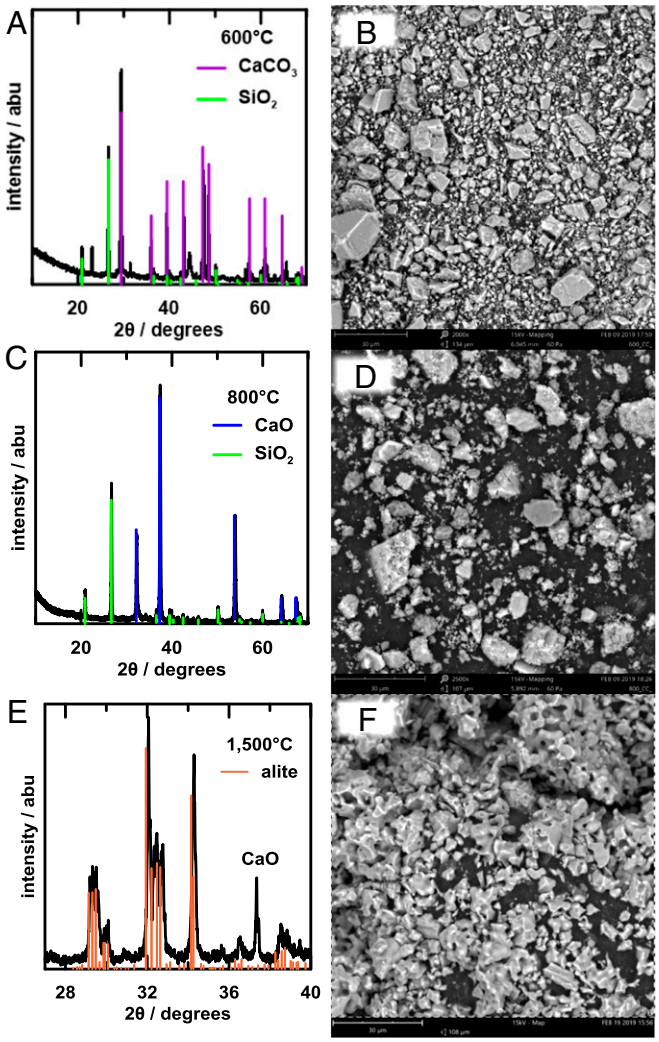

Fig. 7. Synthesis of alite using $CaCO_3$ and SiO_2 shows lower reactivity than with $Ca(OH)_2$. After heating to 600 °C for 2 h in air, (*A*) XRD pattern and (*B*) SEM image show that $CaCO_3$ has not yet decomposed to CaO. After heating to 800 °C for 2 h in air, the XRD pattern (*C*) shows that $CaCO_3$ has decomposed to CaO but has not yet reacted with SiO_2 to form the alite phase. (*D*) SEM image of resulting CaO and SiO_2 powder mixture. After firing to 1,500 °C for 2 h in air, the XRD pattern (*E*) shows a mixture of alite with some residual CaO. (*F*) SEM image of this incompletely reacted mixture.

temperatures without emitting nitrous oxides (NO_x), which have a global warming potential 298 times that of CO_2 on a per-mass basis (40) and also contribute to smog, acid rain, and ozone depletion. Third, the flue gas from oxy-fuel combustion has a higher concentration of CO_2 and fewer NO_x impurities (37, 41), making carbon capture more efficient. In a cement plant using our decarbonation reactor, the O_2/CO_2 gas mixture could therefore be used as oxy-fuel in the high-temperature kiln to lower energy consumption and NO_x emissions. Among other benefits of oxygen enrichment, 1 commercial-scale experiment using 30 to 35% oxygen enrichment resulted in a 25 to 50% increase in cement kiln production (42). Also, oxy-fuel combustion has negligible, if not beneficial, effects on Portland cement clinker quality (39, 43–47).

The concentration of CO_2 in the flue gas from conventional cement kilns is ~25% (48). For chemical absorption with amines, the most technologically mature postcombustion capture method for a combined stream (37, 38), increasing the concentration of CO_2 up to 60% has been shown to decrease heat requirements, solvent regeneration energy, and steam costs of capture (49–53). The gas stream from our decarbonation cell is higher still (67%), which should make amine scrubbing more efficient. However, a greater benefit may be the ability to avoid expensive CCS processes like amine scrubbing altogether. Since here the CO_2 is delivered in a highly concentrated form mixed only with O_2 (and some H_2O vapor), direct capture using the same simple compression processes (54, 55) now used for purified and concentrated CO_2, could be used.

The hydrogen gas produced at the cathode in our decarbonation cell has value as a feedstock in major industries such as ammonia and fertilizer production, oil and gas refining, and process metallurgy and is considered a key component of developing technologies that could decarbonize heavy-duty transportation, aviation, and heating (56, 57). The combined gas streams could also be used in CO_2 utilization processes that produce liquid fuels, such as those that also use hydrogen and produce alcohols.

The hydrogen could also be looped back to support the cement process (Fig. 1). It could be directly combusted to provide heat or electric power back to the cement operation, or the H_2 and O_2/CO_2 gas streams could supply a fuel cell that generates on-site electricity to power the electrochemical reactor or other plant operations such as grinding, mixing, and handling. By using a solid oxide fuel cell (SOFC) (58), which has the highest electrical efficiency of all fuel cell types (60 to 80%) (59), the deleterious effects of the CO_2 on proton exchange membrane fuel cells (60, 61) is averted, and typical SOFC operating temperatures of 500 to 1,000 °C could be readily maintained using heat from the cement kiln (which typically operates at 1,450 to 1,500 °C). Simultaneously, oxygen would be removed from the O_2/CO_2 gas stream, further purifying the CO_2 and simplifying sequestration. Note that this combination of an electrochemical reactor and SOFC creates a regenerative fuel cell (62), which has the ability to store energy if storage of the reactants is provided, and could thereby smooth the intermittency of renewable electricity used to power the cement plant.

The CO_2 stream produced from the decarbonation cell may also have value in applications that up-cycle captured CO_2. CO_2 is already used to enhance oil recovery (EOR) (63, 64) and to make chemicals such as urea, salicylic acid, methanol, carbonates (65), synthetic fuel (via the Fischer–Tropsch process) (66), and synthetic natural gas (via the Sabatier reaction) (67). There is growing interest in finding ways to react CO_2 electrochemically or photochemically to create chemicals and fuels from captured CO_2 using renewable electricity (68). For example, a model plant that uses captured CO_2 to make synfuel has been demonstrated (69).

We also considered the feasibility of operating an electrochemically based cement manufacturing process purely with renewable electricity. Perhaps the least capital-intensive way to use the output gases of the decarbonation reactor is through combustion to heat the cement kiln. We analyzed the energy flows in this configuration; details are given in *SI Appendix*. Assuming a decarbonation reactor operating with 85% coulombic efficiency, an electrolyzer operating at 60 to 75% efficiency, and combustion of the resulting H_2 and O_2 to heat the sintering kiln with 60 to 80% efficiency, the input electrical energy required to make 1 kg of cement is 5.2 to 7.1 MJ. This assumes no energy benefit from the substitution of $Ca(OH)_2$ for $CaCO_3$ in the high-temperature sintering process or other potential benefits such as reduction of capital and energy cost for grinding limestone (given that this function is replaced by chemical dissolution). At 80% efficient combustion of the H_2 and O_2 produced from the decarbonation cell, the thermal energy produced slightly exceeds that required for sintering. If combustion is only 60% efficient, 90% of the thermal energy required for sintering can be supplied from the electrolyzer gases (i.e., ~0.5 MJ/kg of supplemental energy is required). This energy deficit, as well as electric power for supporting operations, could be made up with an excess of electrolyzer capacity above that stoichiometrically needed for decarbonation. This analysis suggests that a renewables-powered electrochemical cement process would not require large amounts of supplemental energy, if any.

An important related question is, of course, the cost of the electrochemically based process. Given the numerous possible configurations discussed above, a complete techno-economic analysis is beyond the scope of this paper. The lifetime cost and

economic return for a complete system or any of its subunits depends on capital cost, efficiency, and durability, as well as the value of the cement and gaseous byproducts. Many of the cost factors are currently unknown; for example, the lifetime cost of the decarbonation reactor will depends on its specific design and performance, none of which have yet been optimized. We therefore limit our techno-economic analysis to a comparison of the energy cost of the electrochemical process with its coal-fired counterpart. The 5.2 to 7.1 MJ/kg cement estimated for the electrochemical process does exceed the energy required for the conventional cement process in the average US kiln, which is 4.6 MJ/kg (70). At a coal price of $61 per ton (for bituminous coal) (71), the energy cost for the conventional process is ~$28 per ton of cement, which is 25% of the average US cement selling price of $113 per metric ton (13). The corresponding cost for the electrochemical process naturally depends on the price of electricity and could in some instances be zero or even negative if obtained from renewable resources. However, for electricity costs of $0.02, $0.04, and $0.06 per kW·h, and assuming an energy requirement for the electrochemical process of 6 MJ/kg, which is in the middle of our estimated range, the energy cost is $35, $60, and $100 per ton of cement, respectively. This suggests that, in the absence of other considerations, the electrochemical process would be cost-competitive with conventional plants (~$28 per ton of cement) if electricity is available at <$0.02 per kW·h. Note that the wholesale cost of wind electricity is now at or slightly below $0.02 per kW·h across much of the interior of the United States (72). We assume that wind electricity will be available at this price for the proposed cement plants, for example from a colocated wind farm.

However, this cost comparison neglects the cost of carbon capture and sequestration, which for amine scrubbing of conventional cement flue gas has been estimated to be on the order of $91 per ton (50). In the electrochemical sequence modeled above, where electrolytic H_2 is combusted to heat the kiln, the cost of directly capturing CO_2 from the O_2/CO_2 stream exhibiting the decarbonation reactor should be less than $40 per ton (50). This would swing net energy costs in favor of the electrochemical process, in an environment where policies require carbon remediation, and where low-cost renewable electricity is available.

Finally, the water intensity of such an electrolyzer-based process should be considered. Each kilogram of cement made using the proposed decarbonation cell would require 0.4 kg of water; this means that the average US kiln, producing 1,800 tons of cement per day, would require ~760 tons of water per day. However, half of this water would be recovered upon the dehydration of $Ca(OH)_2$. If H_2 was used to fuel the kiln, the other half of the water could be condensed from the flue gas. In principle, all of the water used for electrolysis could be recycled.

Conclusions

We propose and demonstrate an electrochemically based cement synthesis process in which $CaCO_3$ is decarbonated and $Ca(OH)_2$ is precipitated in the pH gradient produced by a neutral-water electrolyzer, while concentrated gas streams of H_2 and O_2/CO_2 are simultaneously produced. The fine powder $Ca(OH)_2$ is used to synthesis phase-pure alite, the majority cementitious phase in ordinary Portland cement. The concentrated gas streams from this process may be used synergistically with other processes under development for sustainable industrial technologies. Among several alternatives, the CO_2 may be directly captured and sequestered; the H_2 and/or O_2 may be used to generate electric power via fuel cells or combustors; the O_2 may be used as a component of oxy-fuel to further lower CO_2 and NO_x emissions from the cement kiln; or the output gases may be used to synthesize value-added products such as liquid fuels. Our laboratory-scale prototype decarbonation reactors are shown to be capable of operating with near-theoretical coulombic efficiency, wherein every 2 protons produced at the anode during electrolysis dissolves 1 $CaCO_3$ formula unit. Under such conditions, the electrolytic hydrogen produced, if combusted, can supply most or all of the thermal energy required in high-temperature sintering of the cement. These results suggest a pathway to cost-competitive emissionless cement manufacturing wherein all energy is supplied by renewable electricity.

Materials and Methods

Decarbonation Cells. Custom-designed H-cells were fabricated by James Glass, Inc. The electrolyte was 1 M $NaClO_4$ or $NaNO_3$ (Sigma-Aldrich, ≥98%) dissolved in deionized water. These electrolytes were chosen because their calcium salts are soluble, and because they do not decompose at high voltage. Both electrodes were made from platinum: a rod at the cathode, and a wire at the anode (MW-1032; BASi). Platinum was chosen because it has a high catalytic activity for hydrogen and oxygen evolution in both acid and base. Alternative low-cost electrode materials might include Ni, Cu, or stainless steel for the cathode (pH 12.5) and Al, Sn, or Pb for the anode (pH 6). $CaCO_3$ powder (Sigma-Aldrich, ≥99%) was added to the anode compartment. Filter paper (28310-015, particle retention 5 μm; VWR) was used as the porous separator. Potentiostatic experiments were conducted using a Bio-Logic Science Instruments VMP3 potentiostat. All tests were done at room temperature.

XRD Characterization. XRD patterns were collected using a PANalytical X'Pert PRO XRPD, using Cu radiation and a vertical circle theta:theta goniometer with a radius of 240 mm. The default configuration of this instrument is in Bragg–Brentano geometry with a high-speed high-resolution X'Celerator position-sensitive detector, using the Open Eulerian Cradle sample stage. XRD data were analyzed using Highscore, version 4.7.

SEM Characterization. SEM imaging and compositional analysis of the samples was conducted using a Phenom XL instrument equipped with an energy-dispersive X-ray detector (nanoScience Instruments), operating at 10-kV accelerating voltage for imaging and 15 kV for energy-dispersive X-ray spectroscopy analysis.

BET Characterization. A Quantachrome Instruments NOVA 4000E (Anton Paar QuantaTech) was used to perform multipoint BET analysis of powder specific surface areas.

Alite Synthesis. Electrochemically precipitated $Ca(OH)_2$ or $CaCO_3$ (Sigma-Aldrich, ≥99%) was mixed with SiO_2 (99.5%, 2 μm; Alfa Aesar) in a 3:1 molar ratio. The powders were mixed into a slurry with ethanol then dried. The resulting well-mixed powders were pressed into pellets. The pellets were placed in platinum crucibles and heated at 2 °C per min to 1,500 °C in a muffle furnace (Thermolyne F46120-CM). The temperature was held at 1,500 °C for 2 h, then the pellets were furnace-cooled by turning off the power. The resulting powders were confirmed to be alite by XRD.

ACKNOWLEDGMENTS. This publication is based on work funded by the Skolkovo Institute of Science and Technology (Skoltech), "Center for Research, Education and Innovation for Electrochemical Energy Storage" program under contract 186-MRA. L.D.E. acknowledges support from the Banting Postdoctoral Fellowships program, administered by the Government of Canada. We thank Isaac Metcalf, Nathan Corbin, Kindle Williams, and Karthish Manthiram (Massachusetts Institute of Technology) for experimental assistance; Muhammad Adil and 24 M Technologies, Inc., for performing the BET measurements; and Form Energy, Inc., for providing access to the Phenom XL SEM. This work made use of the Shared Experimental Facilities supported in part by the Materials Research Science and Engineering Centers Program of the National Science Foundation under award DMR-1419807.

1. S. J. Davis *et al*., Net-zero emissions energy systems. *Science* **360**, eaas9793 (2018).
2. F. W. Geels, B. K. Sovacool, T. Schwanen, S. Sorrell, Sociotechnical transitions for deep decarbonization. *Science* **357**, 1242–1244 (2017).
3. M. Åhman, L. J. Nilsson, B. Johansson, Global climate policy and deep decarbonization of energy-intensive industries. *Clim. Policy* **17**, 634–649 (2017).
4. A. Majumdar, J. Deutch, Research opportunities for CO2 utilization and negative emissions at the gigatonne scale. *Joule* **2**, 805–809 (2018).
5. Intergovernmental Panel on Climate Change, *Climate Change 2014: Mitigation of Climate Change: Working Group III Contribution to the Fifth Assessment Report of the Intergovernmental Panel on Climate Change*, O. Edenhofer, Ed. (Cambridge University Press, New York, 2014).
6. IRENA, Renewable power generation costs in 2017 (International Renewable Energy Agency, Abu Dhabi, 2018). https://www.irena.org/-/media/Files/IRENA/Agency/Publication/2018/Jan/IRENA_2017_Power_Costs_2018.pdf. Accessed 16 January 2019.
7. B. Pierpont, D. Nelson, A. Goggins, D. Posner, Flexibility: The path to low-carbon, low-cost electricity grids (Climate Policy Initiative, 2017). https://climatepolicyinitiative.org/wp-content/uploads/2017/04/CPI-Flexibility-the-path-to-low-carbon-low-cost-grids-April-2017.pdf. Accessed 18 January 2019.

8. M. J. Orella, Y. Román-Leshkov, F. R. Brushett, Emerging opportunities for electrochemical processing to enable sustainable chemical manufacturing. *Curr. Opin. Chem. Eng.* **20**, 159–167 (2018).
9. A. Allanore, Contribution of electricity to materials processing: Historical and current perspectives. *JOM* **65**, 130–135 (2013).
10. S. Licht *et al*., STEP cement: Solar thermal electrochemical production of CaO without CO2 emission. *Chem. Commun. (Camb.)* **48**, 6019–6021 (2012).
11. S. Licht, Co-production of cement and carbon nanotubes with a carbon negative footprint. *J. CO2 Util.* **18**, 378–389 (2017).
12. H. F. W. Taylor, *Cement Chemistry* (Thomas Telford Publishing, London, ed. 2, 1997).
13. Mineral Commodities Summary 2018 (U.S. Government Publishing Office, Washington, DC, 2018). https://minerals.usgs.gov/minerals/pubs/mcs/2018/mcs2018.pdf. Accessed 16 January 2019.
14. J. Lehne, F. Preston, Making concrete change; innovation in low-carbon cement and concrete (Chatham House) (2018). https://www.chathamhouse.org/sites/default/files/publications/research/2018-06-13-making-concrete-change-cement-lehne-preston.pdf#CHHJ6042-Cement-report-180611.indd%3A.18769%3A4601. Accessed 11 January 2019.
15. Concrete CO2 Fact Sheet, (National Ready Mixed Concrete Association, Silver Spring, MD, 2012). https://www.nrmca.org/sustainability/CONCRETE%20CO2%20FACT%20SHEET%20FEB%202012.pdf. Accessed 11 January 2019.
16. International Energy Agency, Technology roadmap - low-carbon transition in the cement industry (International Energy Agency, Paris, France, 2018). https://www.iea.org/publications/freepublications/publication/TechnologyRoadmapLowCarbonTransitionintheCementIndustry.pdf. Accessed 16 January 2019.
17. International Energy Agency, Global status report 2017: Towards a zero-emission, efficient, and resilient buildings and construction sector (International Energy Agency, 2017). https://www.worldgbc.org/sites/default/files/UNEP%20188_GABC_en%20%28web%29.pdf. Accessed 26 February 2019.
18. M. S. Imbabi, C. Carrigan, S. McKenna, Trends and developments in green cement and concrete technology. *Int. J. Sustainable Built Environ.* **1**, 194–216 (2012).
19. C. Chen, G. Habert, Y. Bouzidi, A. Jullien, Environmental impact of cement production: Detail of the different processes and cement plant variability evaluation. *J. Clean. Prod.* **18**, 478–485 (2010).
20. A. Hasanbeigi, L. Price, E. Lin, Emerging energy-efficiency and CO2 emission-reduction technologies for cement and concrete production: A technical review. *Renew. Sustain. Energy Rev.* **16**, 6220–6238 (2012).
21. R. Snellings, Assessing understanding and unlocking supplementary cementitious materials. *RILEM Tech. Lett.* **1**, 50–55 (2016).
22. Calera Corporation, www.calera.com/beneficial-reuse-of-co2/index.html. Accessed 28 May 2019.
23. Blue Planet, Ltd., www.blueplanet-ltd.com/#technology. Accessed 28 May 2019.
24. CarbonCure Technologies Inc., https://www.carboncure.com/technology. Accessed 28 May 2019.
25. Q. Li *et al*., A novel strategy for carbon capture and sequestration by rHLPD processing. *Front. Energy Res.* **3**, 53 (2016).
26. J. R. Rumble, Ed., *Handbook of Chemistry and Physics* (CRC Press, Cleveland, OH, ed. 99, 2018).
27. G. H. Rau, CO2 mitigation via capture and chemical conversion in seawater. *Environ. Sci. Technol.* **45**, 1088–1092 (2011).
28. G. H. Rau, Electrochemical splitting of calcium carbonate to increase solution alkalinity: Implications for mitigation of carbon dioxide and ocean acidity. *Environ. Sci. Technol.* **42**, 8935–8940 (2008).
29. G. H. Rau, K. Caldeira, Enhanced carbonate dissolution: A means of sequestering waste CO2 as ocean bicarbonate. *Energy Convers. Manage.* **40**, 1803–1813 (1999).
30. G. H. Rau, H. D. Willauer, Z. J. Ren, The global potential for converting renewable electricity to negative-CO 2 -emissions hydrogen. *Nat. Clim. Chang.* **8**, 621–625 (2018).
31. A. Dowling, J. O'Dwyer, C. C. Adley, Lime in the limelight. *J. Clean. Prod.* **92**, 13–22 (2015).
32. J. A. Madrid, M. Lanzón, Synthesis and morphological examination of high-purity Ca(OH)2 nanoparticles suitable to consolidate porous surfaces. *Appl. Surf. Sci.* **424**, 2–8 (2017).
33. G. Mascolo, B. Marchese, G. Frigione, R. Sersale, Influence of polymorphism and stabilizing ions on the strength of alite. *J. Am. Ceram. Soc.* **56**, 222–223 (1973).
34. I. Odler, S. Abdul-Maula, Polymorphism and hydration of tricalcium silicate doped with ZnO. *J. Am. Ceram. Soc.* **66**, 1–04 (1983).
35. L. Ševula, J. Petrovič, Hydration of polymorphic modification C3S. *Cement Concr. Res.* **11**, 183–190 (1981).
36. M. B. Ali, R. Saidur, M. S. Hossain, A review on emission analysis in cement industries. *Renew. Sustain. Energy Rev.* **15**, 2252–2261 (2011).
37. M. Voldsund *et al*., Comparison of technologies for CO2 capture from cement production—Part 1: Technical evaluation. *Energies* **12**, 559 (2019).
38. L.-M. Bjerge, P. Brevik, CO2 capture in the cement industry, norcem CO2 capture project (Norway). *Energy Procedia* **63**, 6455–6463 (2014).
39. F. Zeman, Oxygen combustion in cement production. *Energy Procedia* **1**, 187–194 (2009).
40. G. Lammel, H. Graßl, Greenhouse effect of NOX. *Environ. Sci. Pollut. Res. Int.* **2**, 40–45 (1995).
41. F. Carrasco-Maldonado *et al*., Oxy-fuel combustion technology for cement production – state of the art research and technology development. *Int. J. Greenh. Gas Control* **45**, 189–199 (2016).
42. World Business Council for Sustainable Development, Development of state of the art techniques in cement manufacturing: Trying to look ahead. https://www.wbcsd.org/Sector-Projects/Cement-Sustainability-Initiative/Resources/Development-of-State-of-the-Art-Techniques-in-Cement-Manufacturing. Accessed 22 February 2019.
43. F. Zeman, K. Lackner, (2008) "The reduced emission oxygen kiln: A white paper report for the cement sustainability initiative of the World Business Council on Sustainable Development (Report No. 2008.01, Lenfest Center for Sustainable Energy, Columbia University, New York).
44. O. Marin, O. Charon, J. Dugue, S. Dukhan, W. Zhou, Simulating the impact of oxygen enrichment in a cement rotary kiln using advanced computational methods. *Combust. Sci. Technol.* **164**, 193–207 (2001).
45. L. Zheng, T. P. Hills, P. Fennell, Phase evolution, characterisation, and performance of cement prepared in an oxy-fuel atmosphere. *Faraday Discuss* **192**, 113–124 (2016).
46. Y. Q. Liu *et al*., Experimental study on improving cement quality with oxygen-enriched combustion technology. *IOP Conf. Series Mater. Sci. Eng.* **103**, 012030 (2015).
47. C. B. Leger, Oxygen lancing for production of cement clinker (1996). https://patents.google.com/patent/US5572938/en. Accessed 17 January 2019.
48. D. J. Barker, S. A. Turner, P. A. Napier-Moore, M. Clark, J. E. Davison, CO_2 capture in the cement industry. *Energy Procedia* **1**, 87–94 (2009).
49. L. Dubois, S. Laribi, S. Mouhoubi, G. De Weireld, D. Thomas, Study of the post-combustion CO2 capture applied to conventional and partial oxy-fuel cement plants. *Energy Procedia* **114**, 6181–6196 (2017).
50. S. O. Gardarsdottir *et al*., Comparison of technologies for CO2 capture from cement production—Part 2: Cost analysis. *Energies* **12**, 542 (2019).
51. A. Lawal, M. Wang, P. Stephenson, G. Koumpouras, H. Yeung, Dynamic modelling and analysis of post-combustion CO2 chemical absorption process for coal-fired power plants. *Fuel* **89**, 2791–2801 (2010).
52. O. Lassagne, L. Gosselin, M. Désilets, M. C. Iliuta, Techno-economic study of CO2 capture for aluminum primary production for different electrolytic cell ventilation rates. *Chem. Eng. J.* **230**, 338–350 (2013).
53. H. Li, G. Haugen, M. Ditaranto, D. Berstad, K. Jordal, Impacts of exhaust gas recirculation (EGR) on the natural gas combined cycle integrated with chemical absorption CO2 capture technology. *Energy Procedia* **4**, 1411–1418 (2011).
54. M. A. Delgado, R. Diego, I. Alvarez, J. Ramos, F. Lockwood, CO2 balance in a compression and purification unit (CPU). *Energy Procedia* **63**, 322–331 (2014).
55. M. Shah *et al*., Near zero emissions oxy-combustion CO2 purification technology. *Energy Procedia* **4**, 988–995 (2011).
56. A. McWilliams, The global hydrogen economy: Technologies and opportunities through 2022 (BCC Research, 2018). https://www.bccresearch.com/report/download/report/EGY055D. Accessed 19 January 2019.
57. International Energy Agency, "Technology roadmap: Hydrogen and fuel cells" (International Energy Agency, 2015).
58. S. C. Singhal, K. Kendall, *High Temperature Solid Oxide Fuel Cells: Fundamentals, Design, and Applications* (Elsevier, Oxford, UK, 2003).
59. O. Schmidt *et al*., Future cost and performance of water electrolysis: An expert elicitation study. *Int. J. Hydrogen Energy* **42**, 30470–30492 (2017).
60. G. J. M. Janssen, Modelling study of CO2 poisoning on PEMFC anodes. *J. Power Sources* **136**, 45–54 (2004).
61. W.-M. Yan *et al*., Degradation of proton exchange membrane fuel cells due to CO and CO2 poisoning. *J. Power Sources* **188**, 141–147 (2009).
62. F. Mitlitsky, B. Myers, A. H. Weisberg, Regenerative fuel cell systems. *Energy Fuels* **12**, 56–71 (1998).
63. S. M. Benson, J. Deutch, Advancing enhanced oil recovery as a sequestration asset. *Joule* **2**, 1386–1389 (2018).
64. M. Blunt, F. J. Fayers, F. M. Orr, Carbon dioxide in enhanced oil recovery. *Energy Convers. Manage.* **34**, 1197–1204 (1993).
65. S. Topham *et al*., "Carbon dioxide" in *Ullmann's Encyclopedia of Industrial Chemistry* (American Cancer Society, 2014), pp. 1–43.
66. X. Li *et al*., Greenhouse gas emissions, energy efficiency, and cost of synthetic fuel production using electrochemical CO2 conversion and the fischer–tropsch process. *Energy Fuels* **30**, 5980–5989 (2016).
67. C. Vogt, M. Monai, G. J. Kramer, B. M. Weckhuysen, The renaissance of the Sabatier reaction and its applications on Earth and in space. *Nat. Catal.* **2**, 188 (2019).
68. H. B. Gray, Powering the planet with solar fuel. *Nat. Chem.* **1**, 7 (2009).
69. D. W. Keith, G. Holmes, D. S. Angelo, K. Heidel, A process for capturing CO2 from the atmosphere. *Joule* **2**, 1573–1594 (2018).
70. Portland Cement Association, Labor-energy input survey. https://www.cement.org/docs/default-source/market-economics-pdfs/more-reports/labor-energy-sample-2.pdf?sfvrsn=6&sfvrsn=6. Accessed 28 February 2019.
71. US Energy Information Administration, Annual survey of coal production and preparation (2017). https://www.eia.gov/coal/annual/pdf/table31.pdf. Accessed 21 February 2019.
72. US Department of Energy, Office of Energy Efficiency and Renewable Energy, 2017 wind technologies market report, https://emp.lbl.gov/wind-technologies-market-report/. Accessed 28 May 2019.